ARMA 12-391

SAND2012-1405C

Laboratory Testing of Waste Isolation Pilot Plant Surrogate Waste Materials

Broome, S.T., Bronowski, D.R., Kuthakun, S.J., and Pfeifle, T.W.
Geomechanics Department, Sandia National Laboratory, Albuquerque, NM, USA
Herrick, C.G.
Performance Assessment and Decision Analysis Department, Sandia National Laboratories, Carlsbad, NM, USA

This paper was prepared for presentation at the 46th US Rock Mechanics / Geomechanics Symposium held in Chicago, IL, USA, 26–29 June 2012.

ABSTRACT:

The present study results are focused on laboratory testing of surrogate waste materials. The surrogate wastes correspond to a conservative estimate of the degraded containers and TRU waste materials emplaced at the WIPP after the 10,000 year regulatory period. Testing consists of hydrostatic, triaxial, and uniaxial strain tests performed on surrogate waste recipes that were previously developed by Hansen et al. (1997) [1]. These recipes can be divided into materials that simulate 50% and 100% degraded waste by weight. The percent degradation indicates the anticipated amount of iron corrosion, as well as the decomposition of cellulosics, plastics, and rubbers (CPR). Axial, lateral, and volumetric strain and axial and lateral stress measurements were made. Two unique testing techniques were developed during the course of the experimental program. The first involves the use of dilatometry to measure sample volumetric strain under a hydrostatic condition. Bulk moduli of the samples measured using this technique were consistent with those measured using more conventional methods. The second technique involved performing triaxial tests under lateral strain control. By limiting the lateral strain to zero by controlling the applied confining pressure while loading the specimen axially in compression, one can maintain a right-circular cylindrical geometry even under large deformations. This technique is preferred over standard triaxial testing methods which result in inhomogeneous deformation or "barreling". Manifestations of the inhomogeneous deformation included non-uniform stress states, as well as unrealistic Poisson's ratios (> 0.5), or those that vary significantly along the length of the specimen. Zero lateral strain controlled tests yield a more uniform stress state, and admissible and uniform values of Poisson's ratio.

1. INTRODUCTION

The Waste Isolation Pilot Plant (WIPP) is a United States (US) Department of Energy (DOE) mined, underground repository, certified by the Environmental Protection Agency (EPA), and designed for the safe management, storage, and disposal of transuranic (TRU) radioactive waste resulting from the United States defense programs. The wastes are emplaced in panels excavated at a depth of 655 m (2,150 ft) in the Permian Salado Formation. Following emplacement of waste and the engineered barrier material MgO, the panels will be isolated from the operational mine using an approved closure system. The repository is linked to the surface by four shafts that ultimately will be decommissioned and sealed.

Performance Assessment (PA) modeling of WIPP performance requires full and accurate understanding of coupled mechanical, hydrological, and geochemical processes and how they evolve through time. The overarching objective of this paper focuses on room closure modeling, specifically the compaction behavior of waste and the constitutive relations to model this behavior. A principal goal of this study is make use of an improved waste constitutive model parameterized to well designed data. Ultimately, any changes in the room closure model or other elements of the underground evolution will require peer review and acceptance by the EPA.

This paper documents hydrostatic, triaxial, and uniaxial strain loading tests conducted on surrogate degraded waste as data required to develop a better constitutive model for WIPP waste behavior. Previous work [1] has been done on different recipes of surrogate material for WIPP Performance Assessment's (PA's) Spallings model parameter evaluation, but these experiments did not provide data needed to correlate volumetric change

to other test parameters. Hansen et al. [1] also performed triaxial tests on surrogate degraded waste mixtures, but only at a limited number of confining pressures were used. A larger range of confining pressures is needed to assist in the modeling efforts for the long term effects of WIPP room closure characteristics.

2. MATERIAL AND SAMPLE PREPARATION

Two unique recipes were used for all samples within this report; 1) a recipe representing a waste state where 50% degradation has occurred and 2) a recipe representing a waste state where 100 % degradation has occurred [1]. The percent degradation indicates the anticipated amount of iron and the amount of cellulosics, plastics, and rubbers (CPR) that are anticipated to be degraded by weight. A description of the constituents for both the 50% and 100% degraded mixtures is presented in Table 1.

Table 1: Ingredient description for 50% and 100% degraded specimens surrogate waste mixtures from [1].

Percent by weight of materials in test specimens		
Material	50% degraded	100% degraded
Iron, not corroded	18.3%	0.0%
Corroded iron and other metals	44.4%	67.0%
Glass	9.6%	9.2%
Cellulosics + plastics + rubber	6.8%	0.0%
Solidification cements	11.6%	11.0%
Soil	4.8%	4.6%
MgO backfill	0.0%	0.0%
Salt precipitate, corrosion-induced	4.5%	8.3%
Salt precipitate, MgO-induced	0.0%	0.0%
Total batch size	100.0%	100.0%

Once the constituents were prepared as described in Table 1, they were combined into a bowl and saturated with brine. Brine was prepared by combining tap water and crushed WIPP salt in a container and mixed by hand shaking at room temperature until the salt no longer dissolves in the water. Solid pieces of salt are left in the container and the container is periodically shaken during use. Figure 1 shows a batch of 100% degraded material ready for insertion into a sample mould.

3. EXPERIMENTAL METHODS

3.1 Hydrostatic Tests

After the material was saturated and mixed in a bowl, it was put into a cylinder of known volume (1641 cc). Leftover material was discarded. By subtracting the weight of the empty 'volume standard', the weight of the material in the 'volume standard' was then calculated and a pretest density determined by dividing material weight by the volume. Figure 2 shows a saturated 50% recipe contained within the 'volume standard'. A repeatable sample volume was important for hydrostatic testing because of the utilization of dilatometry to measure volumetric strain. Section 4 describes in detail the test method employed to accurately record volumetric strain during a test.

Fig. 1. Batch of 100% degraded material ready for insertion into a sample mould.

Fig. 2. Saturated 50% recipe contained within the 'volume standard' ready for insertion into gum rubber jacket assembly.

A section of gum rubber tubing of nominal 101.6mm (4 inch) inside diameter and 3.18mm (1/8 inch) wall thickness was attached to the unvented specimen end cap using tie wire. A stiff plastic shell was placed around the

outside diameter of the gum rubber. The purpose of the shell was to keep the specimen in a shape that approximated a right circular cylinder. The material (1641 cc) was then put into the gum rubber jacket and the other end cap inserted until brine was detected from the vent port. A felt metal filter was used on the vented end cap. The vented end cap was made so that multiple ports connected to the main external drain port prevented clogging during sample deformation. Figure 3 shows a sample ready for hydrostatic testing and details the components of the assembly.

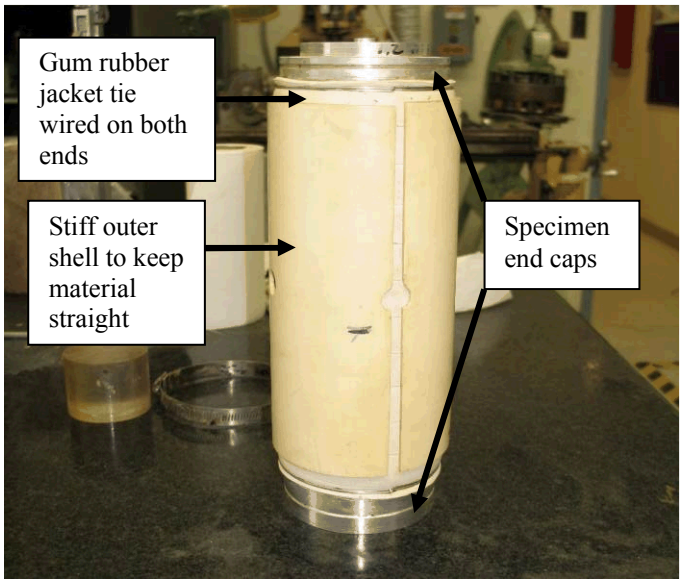

Fig. 3. Sample ready for hydrostatic testing detailing the components of the assembly.

3.2 Triaxial and Uniaxial Strain Tests

Originally, triaxial tests were to be the same specimens used in the hydrostatic tests. The material deforms irregularly during hydrostatic compaction such that the volume of the triaxial sample would not be known by conventional dimensional methods. In addition, upon depressurization, the gum rubber jacket wrinkles and does not facilitate a mounting point for radial measurements. It was decided to pre-compact the material in a split die to 80% of the target confining pressure as illustrated in Figure 4. The die compaction forms the material into a fairly uniform right circular cylinder and allows the use of heat shrink tubing as the jacketing material. During die compaction, the sample is drained from both the top and bottom, and brine was observed along the seam of the die. After die compaction, the sample is unloaded down to approximately 40 pounds of force (180 N). The small preload is left on the material to ensure alignment of the sample stack while the heat shrink jacket is shrunk onto the sample and end caps. Initially, only one jacket was used but after multiple jacket leaks (at confining pressures of 5 MPa and above), all 50% degraded material samples received two heat shrink jackets, while 100% degraded samples always were tested with one jacket.

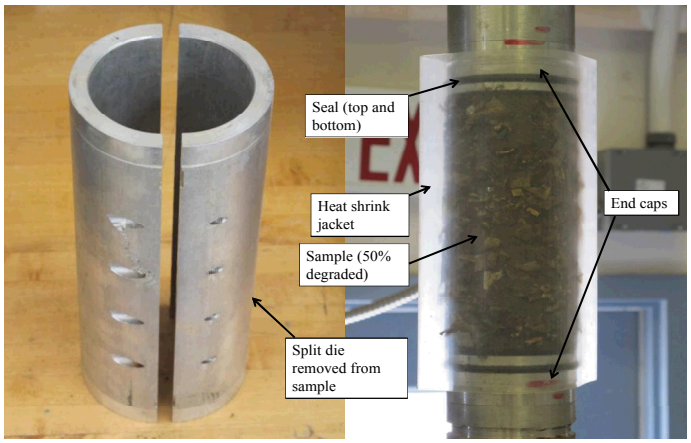

Fig. 4. Split die shown along with die compacted 50% degraded material prior to heat shrink application.

A triaxial/uniaxial strain sample, instrumented with linear variable differential transformers (LVDT's) is shown in Figure 5 and in Figure 6 the sample is mounted on the pressure vessel base and is ready for testing. As shown in Figure 6, the sample is drained from both the top and bottom end caps. The top end cap has a port on the side. This port is connected to the vessel base with a flexible tube. The bottom end cap is ported in the center and connects to the vessel base with a sealed nipple.

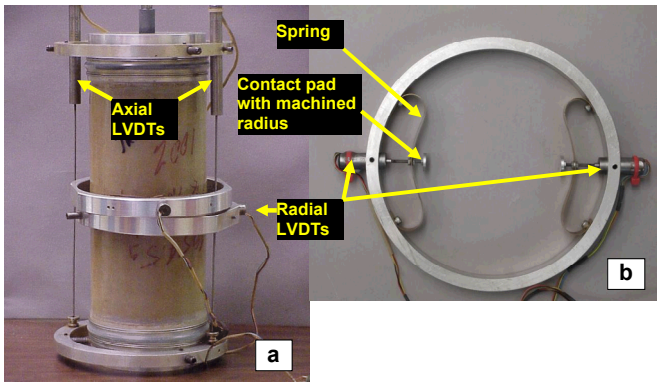

Fig. 5. Typical instrumented triaxial/uniaxial strain test specimen: (a) Axial and radial deformations measured using LVDTs mounted in rings and (b) detail of radial deformation ring.

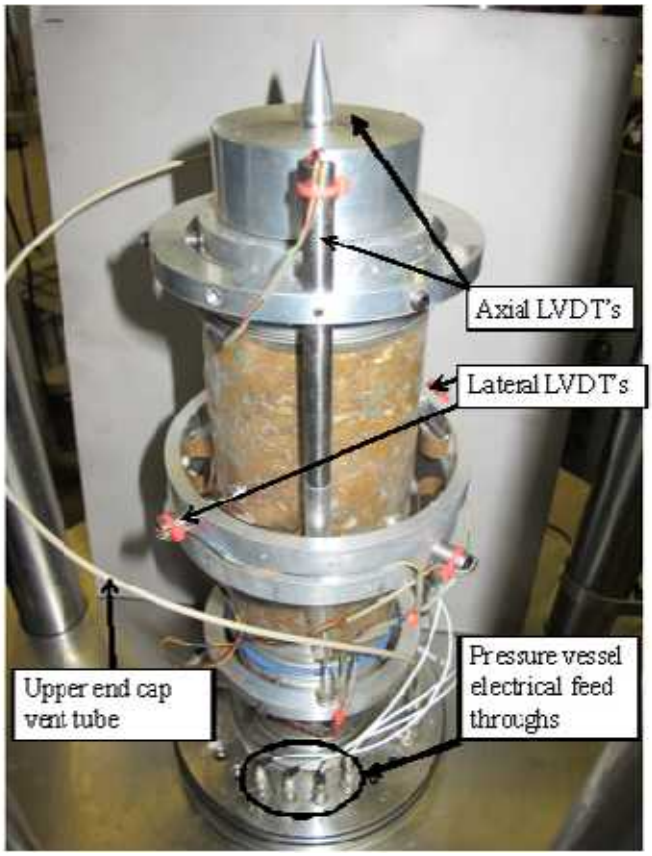

Fig. 6. A triaxial sample (50% degraded material) mounted on the pressure vessel base and ready for testing.

3.3 Test Systems

Three computer-controlled servohydraulic test systems, all manufactured by MTS Systems Corporation (MTS), were used in the testing of the 50% and 100% degraded sample. The systems were selected primarily to match capabilities to the load and confining pressure requirements specified in the test matrix. As shown in Table 2, the primary differences among the test systems were the maximum axial loads and confining pressures that could be applied during a test.

Hydrostatic tests were performed using MTS 0.1 MN and 1.0 MN test systems. The 0.1 MN system comprises a standard two-column load frame, MTS FlexTestTM digital controller, and desktop PC. The system served solely as an intensifier/dilatometer (I/D) (see Figure 7) that ran in parallel with the dedicated I/D mounted near the four-column 1.0 MN frame (Figure 8).

Triaxial and uniaxial strain tests were performed using the MTS 1.0 MN test system shown in Figure 8. For the die compaction phase of these tests (sample pre-compaction), a two-column MTS 1.0 MN Axial/Torsional frame was utilized and is shown in Figure 9.

The standard MTS two and four-column load frames used in this test series are equipped with movable crossheads to accommodate different specimen/equipment geometries. A hydraulic actuator located in the base of the frame is capable of applying axial force over the ranges specified in Table 2 in both tension and compression. Force is measured by an electronic load cell mounted on the crosshead, while the relative displacement of the load actuator is determined from a linear variable differential transformer (LVDT) mounted internal to the actuator housing.

The 100 MPa pressure vessel used for all tests is shown in Figure 10. The burette shown along the side of the pressure vessel was utilized in uniaxial strain tests to determine sample volume at discreet intervals during the test. Section 4 discusses in detail the test method incorporating this measurement technique.

Table 2: Test System Capabilities and Utilization

Test System	Axial Force Range MN (kip)	Confining Pressure Range MPa (ksi)	Utilization
0.1 MN	0 – 0.1 (0 – 22)	NA	Frame served as a hydrostatic I/D run in parallel with 1.0 MN system.
1.0 MN	0 – 1 (0 – 220)	0 – 100 (0 – 15)	All samples tested with a 100 MPa pressure vessel.
1.0 MN AT	0 – 1 (0 – 220)	NA	Die compaction of triaxial and uniaxial strain samples.

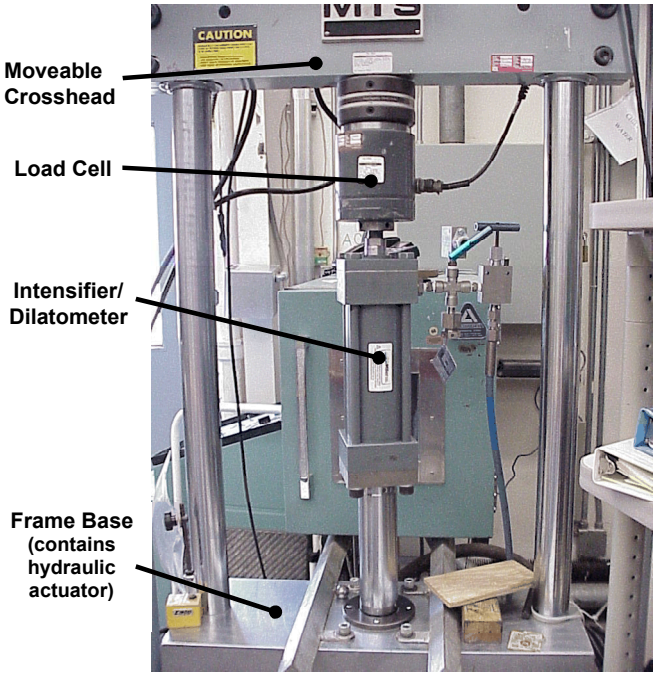

Fig. 7. MTS 0.1 MN Test System used as an intensifier/dilatometer for hydrostatic testing.

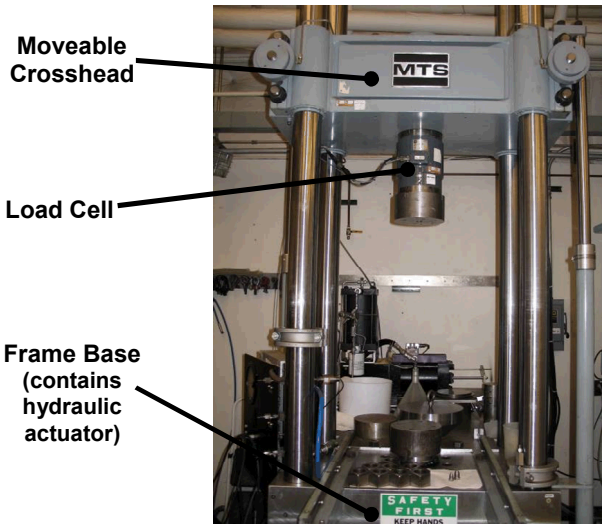

Fig. 8. MTS 1 MN test frame used for hydrostatic, triaxial, and uniaxial strain testing.

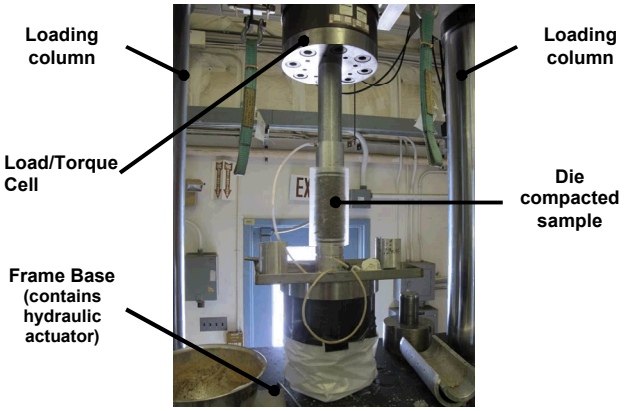

Fig. 9. MTS 1 MN AT test frame used for triaxial and uniaxial strain testing.

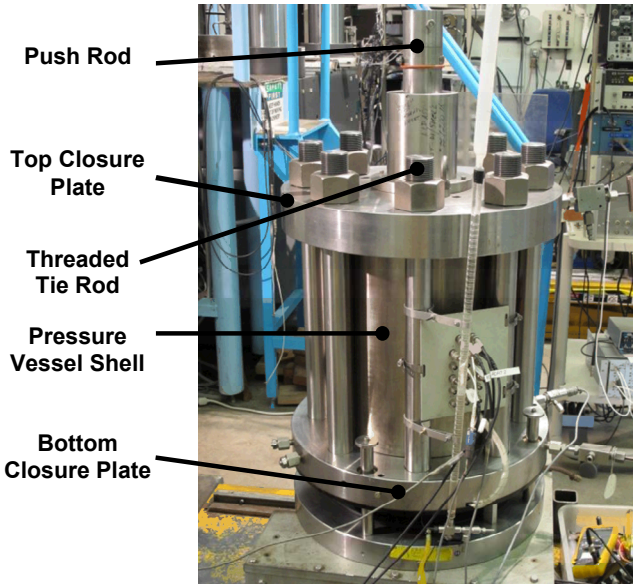

Fig. 10. SBEL 100 MPa pressure vessel used with four-column MTS 1 MN test system.

4. TEST METHODS

4.1 Hydrostatic Tests

Hydrostatic compression testing utilized dilatometry to measure volumetric strain of the sample. In simple terms the process works in the following manner:

- A known volume of test material is placed in a length of rubber tubing
- The tubing ends are plugged using end caps
- The assembly is placed in a pressure vessel and the vessel filled with confining fluid
- The vessel is plumbed to an I/D
- The I/D system produces pressure in the pressure vessel by displacing fluid
- The fluid displacement (volume) is measured
- As pressure compresses the sample material, additional fluid is required to maintain the desired pressure
- Fluid displacement relates to volumetric strain of the sample material

In practice there are several tasks that are critical to the overall process in order to produce reliable/accurate measurements. Fluid volume measured by the dilatometer is not a direct relationship to material compaction. This is due to the complexity of the total test system and how it responds to pressure changes. Some significant considerations are: 1) the fluid itself is compressible, 2) the pressure vessel, test frame, and associated plumbing all strain under pressure and 3) the rubber jacket material compresses. It is not practical to attempt analytical corrections for each contributing component. Instead, total system response will be measured by performing tests on a known volume of well characterized material via a test billet. By this process, a system response baseline will be produced which will then be subtracted from material test data. Figure 11 shows a typical pressure versus volume response for a 100% degraded sample. Both uncorrected and corrected data are shown: uncorrected data includes sample and system deformation and corrected data factors out the system deformation thus showing only sample deformation.

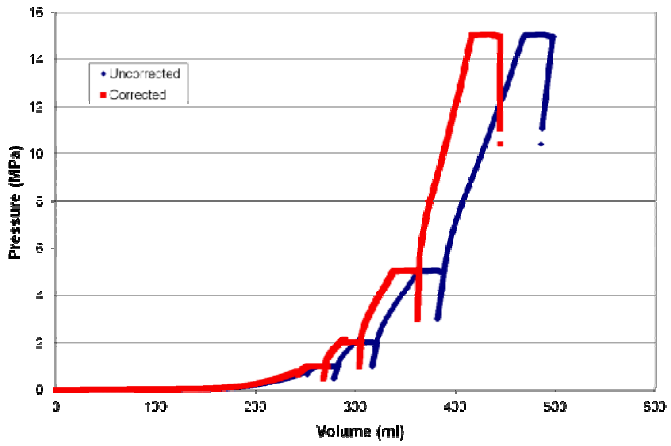

Fig. 11. Typical pressure versus volume response illustrating the effect of system deformation on sample deformation measurements.

In order for the above described process to be reliable, several points are critical: 1) the configuration under which the system response was measured must not change. This includes using the same (or identical) sample assembly hardware and the same initial volume of test material, 2) the same pressure vessel, dilatometers, and all plumbing components, and 3) consistent starting position of dilatometer and vessel pistons and proper system filling and purging. All items relate directly to assuring that the same amount of confining fluid is in the system for every test. A plastic stuffer was inserted into the pressure vessel to remove as much fluid as possible from the system. Using a stuffer makes the system stiffer and increases the accuracy of the volumetric strain data when factoring out the system response from the test data.

Every test must be performed at the same pressurization rate to minimize a difference in heating/cooling effects on the system response test and sample test. All testing used defined pressurization rates to assure that test time periods are consistent.

Hydrostatic tests are performed in two parts. The first part uses the entire system where the 0.1 MN frame is the driving I/D to compact the sample. The 0.1 MN dilatometer is then isolated (valve closed) and testing continues using the 1 MN dilatometer.

Preparation of the system for a test begins with closing the vessel and positioning it in the test frame. The vessel is then filled with confining fluid (tap water with anti corrosive additive). Next, the system drain valve is opened and each I/D is operated to completely empty. Each system vent valve (one near each I/D and one at the top of the pressure vessel) is opened to purge each section of plumbing. Purging continues until no air bubbles are observed from the vent.

Testing begins by operating the 0.1 MN test frame in pressure control mode using programmed rates. Different rates are used throughout the test. Initially, the 0.1 MN I/D is driven to deliver confining fluid to produce a very slow but constant rate of pressure increase. The pressure rate is increased twice during this portion of the test. The initial slow rate(s) are to allow sufficient time for brine to be expelled from the sample via the vent port. The rates were also selected to approximate the shape of a time/pressurization curve if a constant volume displacement rate were used. While more complicated from a programming standpoint, the pressure rate method allows all samples, regardless of material stiffness, to be performed in the same period of time. Additionally, system response tests, which would pressurize quickly using a volume displacement rate, were also performed over the same time period by using this method.

Pressurization rates for the first part of the test (using only the 0.1 MN I/D) are:

- 30 Pa/sec from start of test to 0.1 MPa
- 100 Pa/sec from 0.1 MPa to 0.3 MPa
- 300 Pa/sec from 0.3 MPa to approximately 1.0 MPa

The first part of the test takes 2.13 hours to complete and is terminated (0.1 MN I/D valve closed) when either a fluid volume displacement of 400.0 ml is obtained or a pressure of 1 MPa is reached. If 1 MPa pressure is reached first, the 1 MN frame is operated to back out the vessel piston until the full 400.0 ml is delivered from the 0.1 MN I/D. When 400.0 ml of fluid volume displacement is reached then the second part of the test begins using the 1 MN frame.

The second part of the test continues to pressurize the sample to the target pressure (usually 1 MPa) using only the 1 MN frame and I/D. This is performed by running the 1 MN I/D at a pressurization rate of 0.002 MPa/sec until the target pressure is obtained. The sample is then held at this pressure overnight.

After the overnight hold (~16 hours), an unload/reload pressurization cycle is performed using the 1 MN I/D to obtain bulk modulus data at 1 MPa. After the unload/reload loop is performed the pressure is raised to the next hydrostatic pressure level of 2 MPa at 0.002 MPa/sec. The sample is held at 2 MPa overnight and an unload/reload loop performed at 2 MPa the next morning. This process is repeated at 5 and 15 MPa. After the unload/reload loop at 15 MPa, the sample is unloaded completely and the test dissembled. Figure 12 shows a hydrostatic test after testing with the jacket still on the sample and with the jacket removed.

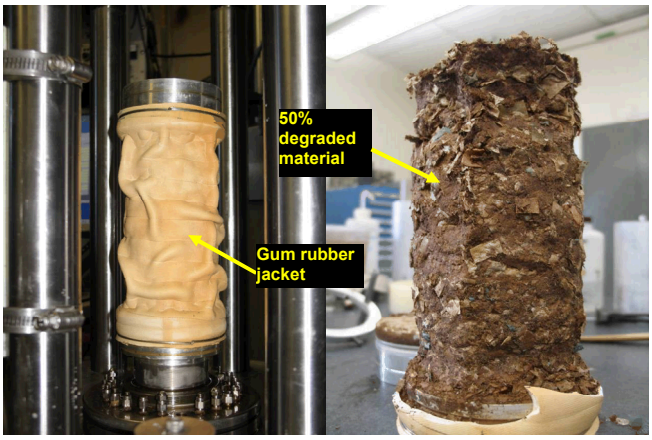

Fig. 12. At left: typical hydrostatic test specimen posttest with vacuum applied to show compaction; at right a specimen after its jacket was removed (50% degraded material).

After four hydrostatic tests were performed the test setup was modified to accommodate pore pressure readings. The decisions to measure pore pressure arose from observed creep during the overnight pressure holds. Understanding whether the creep observed was based on pore pressure or material characteristics would help in the understanding of material behavior at these stress states.

4.2 Triaxial Tests

Figure 12 shows the irregular shape of material after hydrostatic testing. Because of this irregular shape, triaxial compression tests were not possible on posttest hydrostatic material. A die compaction of both 50% and 100% surrogate degraded recipes was used to form right circular cylinders for jacketing and instrumentation for triaxial testing. Section 3.2 details the die compaction process performed on the 1 MN AT load frame.

After the material was die compacted to 80% of the target confining stress, a heat shrink jacket was shrunk on the sample with sealed aluminum end caps. Both end caps were vented and utilized a porous felt metal filter. Axial LVDT's were mounted on the end caps of the sample using aluminum rings with set screws to keep the rings from moving during testing. Radial LVDT's were mounted on either side of the sample center (see Figure 10). The sample was then mounted in the 100 MPa capacity pressure vessel and pressure was increased to the target confining pressure (1, 2, 5, or 15 MPa) at 0.002 MPa/sec. The sample was held at this confining pressure in a hydrostatic stress state overnight (approximately 16 hours).

The following day, an unload/reload loop was performed to obtain bulk modulus data. This is similar to the bulk modulus data obtained from hydrostatic testing with the exception of the way volume strain was measured. With the hydrostatic tests, volumetric strain was determined dilatometrically as discussed in Section 4.1. Volumetric strain for the triaxial tests was determined by combining the output from the sample mounted axial and radial LVDT's. It should be noted that while the triaxial test was held in a hydrostatic stress state overnight, the majority of compaction occurred in a one dimensional stress state (die compaction).

After the bulk modulus loop was performed, the actuator was advanced on the 1 MN test system until the piston made contact with the top of the sample. After contact was made the actuator continued to advance and applied a differential stress to the sample. Confining pressure was held constant for the remainder of the test using feedback control from the pressure sensor and the 1 MN test system I/D. Multiple unload/reload loops were performed to determine Young's modulus and Poisson's ratio as the sample deformed. Samples were typically deformed around 15 to 20% axial strain.

A burette was mounted on the side of the pressure vessel and was used to collect fluid expelled from the sample as it was compacted. The fluid was drained out of the burette after the overnight hydrostatic hold and also at the conclusion of the triaxial test. The fluid was collected and weighed so that the density of the sample could be determined at these stages of the test. The quantity of fluid was known because the fluid level in the burette was always returned to a marked starting level.

After a number of tests were performed it was discovered that Poisson's ratio (ν) increased as axial strain increased. Although triaxial samples were vented from both ends, there was concern that pore pressure was building up inside the sample and causing the unrealistically high ν values (above 0.5). Two samples were tested (one 50% and one 100% degraded recipes) using slower pressure and axial strain rates. The confining pressure rate was reduced by 80% to 0.0004 MPa/sec (previously 0.002 MPa/sec) and the axial displacement rate was reduced to 0.0000175 in/sec (previously 0.00035 in/sec). The slow axial strain rate is 20 times slower than previous tests. No noticeable change in sample behavior was observed.

Sample barreling was considered a possibility and investigated by mounting one radial LVDT ring at approximately 25% from the top of the sample and another at sample mid-height (as opposed to both radial LVDT's mounted near sample mid-height). Calculating ν from the LVDT at sample mid- height revealed similar high values (over 0.5) as seen before but using the other radial LVDT (25% from the top of the sample) gave values of nearly half of that from the mid-height radial LVDT. While the tests performed thus far provide good Young's modulus and axial deformation data useful for failure envelope modeling, a different approach was deemed necessary to understand lateral sample behavior. Testing a sample in a uniaxial strain configuration would

allow determination of v as a function of density. This method is outlined in sections 5.3 and 6.3.

4.3 Uniaxial Strain Tests

Six uniaxial strain tests were performed (three on each recipe). Uniaxial strain tests are prepared identically to triaxial compression tests. The method for applying hydrostatic stress is also identical to that employed for triaxial testing. When the actuator is inserted into the pressure vessel and begins to apply axial differential stress, confining pressure is increased to maintain a zero lateral strain condition. The control for the zero lateral strain condition is the radial LVDT mounted at sample mid-height. The other radial LVDT is mounted 25% from the top of the sample (same mounting arrangement as for the triaxial compression test when sample barreling was investigated).

The frame actuator was displaced at a rate that allowed the test to be run for approximately 8 hours. The slow rate was desired because of the anticipated large increases in confining pressure to maintain the zero lateral strain condition and to allow proper drainage of brine from the sample. Another change from the triaxial tests was the measurement of brine expelled from the test just before each unload/reload loop was performed. These measurements of brine were in addition to those discussed in the previous section (post hydrostatic hold and post triaxial test). A new burette was used with graduation marks along the entire length allowing a list of burette levels to be recorded during testing. The brine measurements allowed the density to be calculated and plotted as a function of Young's modulus and Poisson's ratio.

5. DATA REDUCTION

Data obtained from the data acquisition system (DAS) during each test included axial force, confining pressure, pore pressure, axial and radial displacements (or volume strain from dilatometry), and elapsed time. All data except for time were collected in voltage form. These data were transferred to individual Microsoft® Excel spreadsheets where they were converted to engineering units of stress and strain which were subsequently plotted in graphical form for visual display and analysis.

During this data reduction, the traditional rock mechanics sign convention was used in which compressive stresses and strains were taken as positive quantities and tensile stresses and strains were taken as negative quantities.

5.1 Hydrostatic Tests

Data was collected from all hydrostatic compression tests to facilitate creation of a pressure versus volumetric strain plot. Pressure is collected directly from the DAS in voltage form and converted to pressure units (MPa) using calibration sensitivity values. Volume was determined by measuring (in voltage) the I/D's movement and converting to units of milliliters using calibration sensitivity values. Discussed in Section 4, the volume measured included sample deformation and system deformation. A system response test that was performed identically to the sample test created a pressure versus volume curve on the system minus the sample. The test sample for the system response test was an aluminum billet of identical volume as a triaxial test specimen. The pressure/volume response of the system was then subtracted from the pressure/volume response of the system plus the sample, therefore isolating the volumetric response of the sample as a function of pressure.

Subtracting out the system deformation was accomplished using two methods. The first method used a look up table to factor out system deformation. A look up table is best used when the response of the system cannot be easily represented by a polynomial best fit curve. Pressure/volume data from the system response test was divided into different groups representing periods of uninterrupted pressure increase. Sample pressure data was then matched to pressure from the system response. That pressure then correlated to a volumetric strain of the system that was subtracted from the sample volume data. The system deformation was typically less than 12% of the sample deformation. The look up table method was used to subtract out system deformation for the entire pressure versus volume curve with the exception of the unload/reload loops.

The second method was used to correct the unload/reload data and took advantage of the accuracy of the fit that a polynomial or linear trendline gave. Figure 13 shows a plot of volume versus pressure data from the system response after the valve on the 0.1 MN I/D was closed (indicating 400 ml of fluid has already been pushed into the pressure vessel).

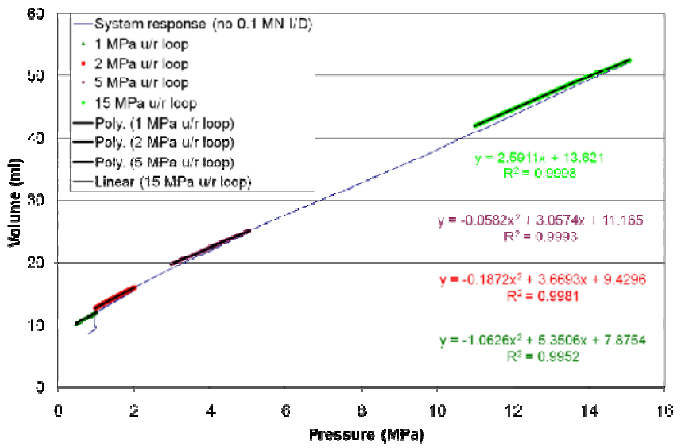

Fig. 13. Volume versus pressure for a system response test. Equations of best fit lines from unload/reload (u/r) data were used to determine bulk modulus data as a function of pressure.

This plot shows unload/reload loops performed at the same pressures where sample unload/reload loops were performed. All equations of the best fit lines show R^2 values at least 0.995 indicating a very good fit. These equations were used to calculate the volume to subtract from the equivalent test pressure.

Both methods described above (look up table and best fit equation) were combined to create a complete pressure versus volumetric strain plot of the sample. This plot and elastic properties derived from it will be presented and discussed in Section 6. Bulk modulus values as a function of confining pressure were determined for both 50% and 100% material. Bulk modulus was calculated from,

$$K = \frac{\sigma_c}{\varepsilon_v} \tag{1}$$

where σ_c is confining pressure and ε_v is volumetric strain.

5.2 Triaxial Tests

Data was collected from all triaxial compression tests to facilitate creation of a differential stress versus axial, lateral, and volume strain plot and allow calculation of bulk modulus prior to starting the triaxial portion of the test. Specifically, the data collected were time, confining pressure, internal force, external force, axial sample displacement, and lateral sample displacements. The bulk modulus was calculated using Equation 1 where ε_v was calculated from,

$$\varepsilon_v = \varepsilon_a + 2\varepsilon_l \tag{2}$$

where ε_a is axial strain and ε_l is lateral strain.

Also, true or Cauchy stress and true or logarithm strain were calculated from the acquired data rather than engineering stresses and strains because of the relatively large deformations measured in the tests. Cauchy stress (σ_a = axial specimen stress and σ_r = radial specimen stress) and true strain (ε_a = axial strain and ε_l = lateral strain) are calculated from,

$$\sigma_a = \frac{F_{sp}^a}{\frac{\pi}{4}\left(D_{sp}^i\right)^2} = \frac{F_{sp}^a}{\frac{\pi}{4}\left(D_{sp}^0 - \Delta D_{sp}\right)^2} \tag{3}$$

$$\sigma_r = \sigma_c \tag{4}$$

$$\varepsilon_a = -\ln\left(\frac{L_{sp}^i}{L_{sp}^o}\right) = -\ln\left(1 - \frac{\Delta L_{sp}}{L_{sp}^o}\right) \tag{5}$$

$$\varepsilon_l = -\ln\left(\frac{D_{sp}^i}{D_{sp}^o}\right) = -\ln\left(1 - \frac{\Delta D_{sp}}{D_{sp}^o}\right) \tag{6}$$

Where:

F_{sp}^a	=	Axial specimen force
D_{sp}^o , D_{sp}^i	=	Original and current specimen diameters, respectively
ΔD_{sp}	=	Change in specimen diameter
L_{sp}^o , L_{sp}^i	=	Original and current specimen lengths, respectively
ΔL_{sp}	=	Change in specimen length
σ_c	=	Confining pressure

5.3 Uniaxial Strain Tests

Data was reduced from the uniaxial strain tests in the same manner as the triaxial compression tests with the exception of calculating axial stress. Axial stress was determined by adding differential stress to confining pressure. This data facilitated plots of confining pressure versus axial stress and differential stress versus axial strain. From these plots, Young's modulus and v can be determined from the following formulae:

From [2],

$$\varepsilon_{11} = \frac{1}{E}(\sigma_{11} - \nu(\sigma_{22} + \sigma_{33})) \tag{7}$$

$$\varepsilon_{22} = \frac{1}{E}(\sigma_{22} - \nu(\sigma_{11} + \sigma_{33})) \tag{8}$$

$$\varepsilon_{33} = \frac{1}{E}(\sigma_{33} - \nu(\sigma_{11} + \sigma_{22})) \tag{9}$$

For uniaxial strain tests conducted under triaxial compression,

$$\sigma_{11} = \sigma_a \tag{10}$$

$$\sigma_{22} = \sigma_{33} = \sigma_r \tag{11}$$

$$\varepsilon_{22} = \varepsilon_{33} = 0 \tag{12}$$

From either Eq 8 or 9 above, with substitution of Eqs 10 – 12,

$$0 = \frac{1}{E}(\sigma_r - \nu(\sigma_a + \sigma_r)) \tag{13}$$

And by re-arranging

$$\sigma_r = \left(\frac{\nu}{1-\nu}\right)\sigma_a \tag{14}$$

For a uniaxial strain test with unload/reload loops, Eq 14 suggests the slopes of the σ_r versus σ_a plots for the unload/reload curves will equal [$\nu/(1-\nu)$] from which ν can be calculated directly.

If Eq 8 is subtracted from Eq 7 and the substitutions of Eqs 10-12 are made, then

$$\varepsilon_a - \varepsilon_r = \varepsilon_a - 0 = \frac{1}{E}(\sigma_a - 2\nu\sigma_r) - \frac{1}{E}(\sigma_r - \nu(\sigma_r + \sigma_a)) \tag{15}$$

$$\varepsilon_a = \frac{1}{E}(\sigma_a - 2\nu\sigma_r - \sigma_r + \nu\sigma_r + \nu\sigma_a) \tag{16}$$

$$\varepsilon_a = \frac{1}{E}((\sigma_a + \nu\sigma_a) - (\sigma_r + \nu\sigma_r)) \tag{17}$$

$$\varepsilon_a = \frac{1}{E}(\sigma_a(1+\nu) - \sigma_r(1+\nu)) \tag{18}$$

$$\varepsilon_a = \frac{1+\nu}{E}(\sigma_a - \sigma_r) \tag{19}$$

$$\sigma_a - \sigma_r = \left(\frac{E}{1+\nu}\right)\varepsilon_a \tag{20}$$

Again for a uniaxial strain test with unload/reload loops, Eq 20 suggests the slopes of the ($\sigma_a - \sigma_r$) versus ε_a plots for the unload/reload curves will equal [$E/(1+\nu)$]. Since ν is determined directly from Eq 14, then E can be determined from Eq 20. Note: ($\sigma_a - \sigma_r$) is simply the measured stress difference during the test.

6. RESULTS

6.1 Hydrostatic Tests

Four hydrostatic tests were performed on the 50% degraded material and five tests were performed on the 100% degraded material. That the results were consistent from sample to sample was apparent by both posttest observation and from the pressure versus volume response. Figure 14 shows all posttest hydrostatic samples of both 50% and 100% degraded recipes.

Table 3 summarizes the results of all hydrostatic tests. Bulk modulus values in Table 4 are calculated from two points; the upper point is where the reload data intersects the unload data and the lower point is the lowest pressure measured during unloading. Using these two points effectively averages the slope of the u/r loop. Bulk modulus values labeled with an "N" indicate that value was not measured either because of a jacket leak or in the case of sample WC-HC-50-04, the pressure was ramped directly to 5 MPa without u/r loops performed at 1 MPa and 2 MPa. Pore pressure measurements were made on the last two and last three 50% and 100% degraded specimens, respectively. These measurements will be discussed in further detail later in this section.

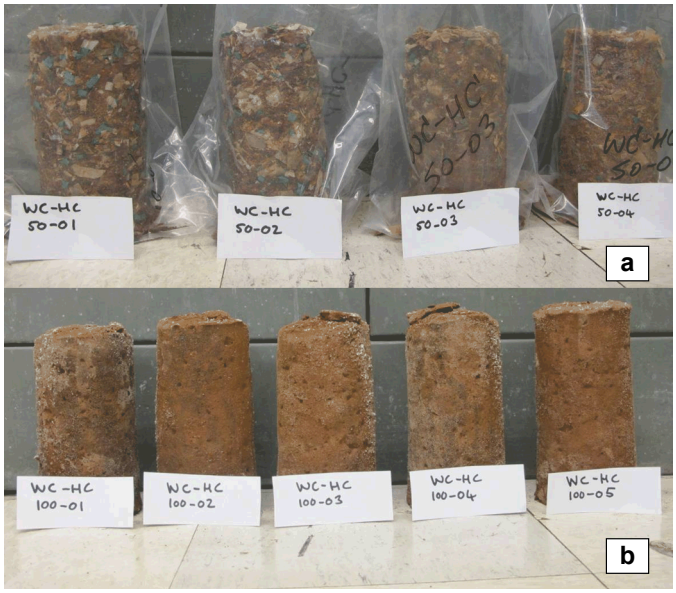

Fig. 14. Posttest 50% (a) and 100% (b) degraded hydrostatic compression samples.

Combined pressure versus engineering volume strain response of 50% and 100% degraded samples is shown in Figures 15 and 16, respectively, and illustrates the consistency of samples with like material types. Represented in Table 4 by bulk modulus values and Figures 15 and 16 by engineering volume strain, 100% degraded specimens are stiffer than 50% degraded specimens. A large percentage of sample deformation occurs during initial pressurization up to 1 MPa. Above 1 MPa, the material begins to stiffen and after 5 MPa confining pressure, little compaction is observed up to the maximum confining pressure of 15 MPa.

A typical response of pore pressure to an increase in sample confining pressure is shown in Figure 17. Pore pressure is multiplied by 100 so it can be represented on the same vertical axis as confining pressure. Interest in measuring pore pressure arose from the concern of sample creep.

Sample creep can either be from creep of the material itself, continued compaction of the material due to a buildup of pore pressure within the sample, or a combination of both. Because pore pressure measurements indicate an overall small but measureable decay in pore pressure with time after an increase in confining pressure, pore pressure is likely a contributing factor to sample creep. Figure 18 shows a plot where

pore pressure is subtracted from confining pressure and compared against confining pressure versus volume strain response of sample WC-HC-50-03.

Table 3: Summary of results from hydrostatic tests.

		Bulk modulus (MPa)				
Sample	Material	K @ 1MPa	K @ 2MPa	K @ 5MPa	K @ 15MPa	Comments
WC-HC-50-01	50%	274	577	1931	11350	
WC-HC-50-02	50%	239	680	2146	4703	
WC-HC-50-03	50%	283	749	2510	N	Jacket leak at 15MPa
WC-HC-50-04	50%	N	N	2194	4690	Pressure ramped directly to 5MPa
WC-HC-100-01	100%	460	1083	2186	32640	
WC-HC-100-02	100%	482	1134	2174	N	Pressure vessel leaked above 5MPa
WC-HC-100-03	100%	509	1427	2786	18720	Pore pressure tube pinched off above 5MPa
WC-HC-100-04	100%	463	1399	3490	N	Pressure vessel leaked
WC-HC-100-05	100%	653	1396	3130	5982	

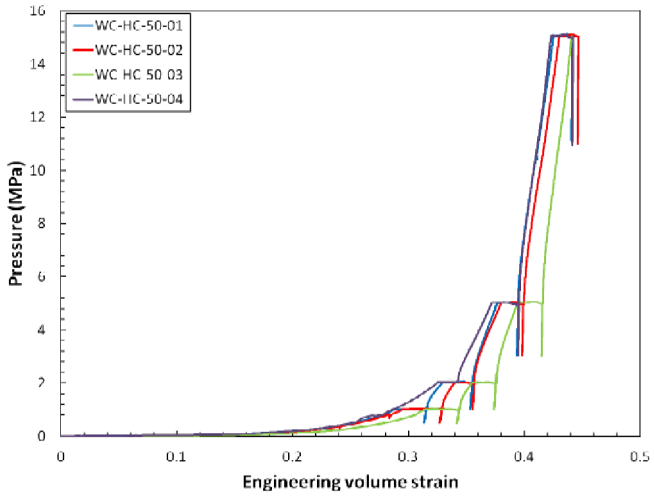

Fig. 15. Pressure versus engineering volume strain for all 50% degraded samples.

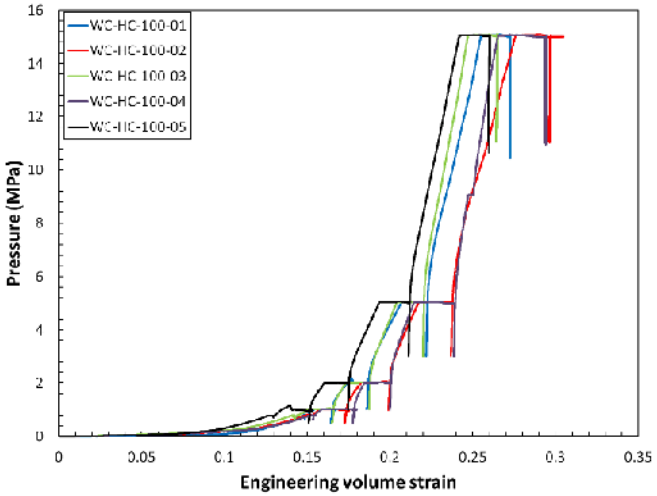

Fig. 16. Pressure versus engineering volume strain for all 100% degraded samples.

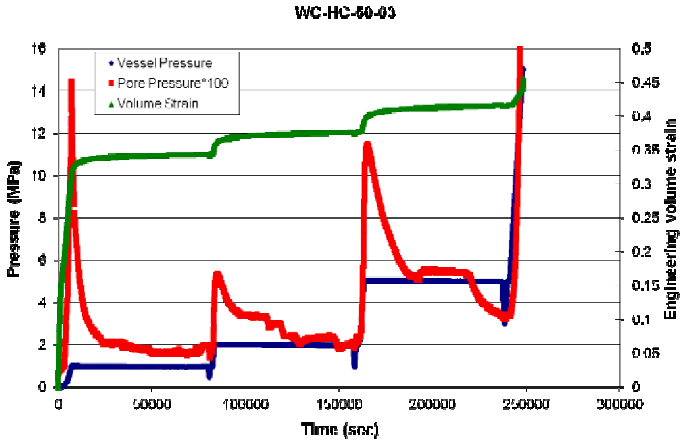

Fig. 17. Pressure, pore pressure and engineering volume strain versus time for sample WC-HC-50-03. Sample jacket leaked at 15 MPa resulting in spike in pore pressure.

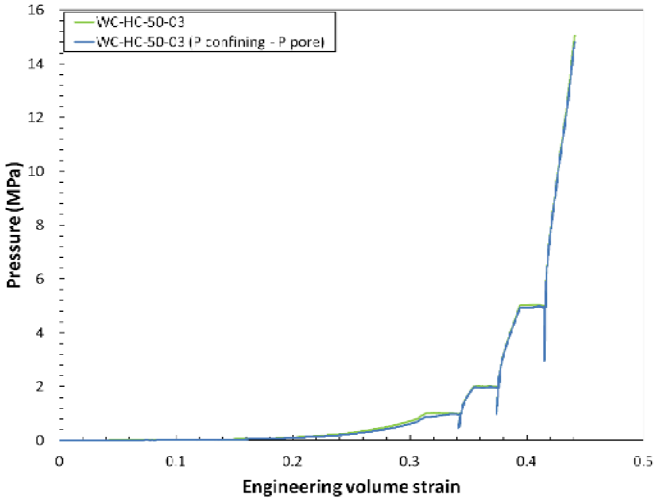

Fig. 18. $P_{confining}$ and $P_{confining}$-P_{pore} versus engineering volume strain for sample WC-HC-50-03. Sample jacket leaked at 15 MPa resulting in no overnight hold data at this pressure.

As the sample is held overnight at 1, 2, and 5 MPa (15 MPa overnight hold was not achieved on this sample due to a jacket leak), $P_{confining}$-P_{pore} is lower than $P_{confining}$

initially. After a few hours, $P_{confining}$-P_{pore} reaches nearly the same value as $P_{confining}$ indicating a reduction of pore pressure as seen in Figure 17. Only one measurement of pore pressure was made and the sample was vented from the other end (pore pressure = 0 at the vented end). The measured values of pore pressure are nearly two orders of magnitude smaller than confining pressure and it remains unclear of the extent that sample creep is influenced by pore pressure.

As shown in Figure 2, the volume and weight of starting material for each sample is known. By subtracting the volume reduction measured during testing and weighing the sample posttest, both pre- and posttest sample densities are known. In the case of sample WC-HC-50-03, the posttest density is high likely due to a jacket leak that added confining fluid to the sample mass. Samples WC-HC-100-02 and WC-HC-100-04 also have higher than average posttest density values and are likely a result of the small pressure vessel leak detected during both of these tests. A pressure vessel leak would give a false volume measurement yielding an inaccurate posttest density measurement. Table 4 lists pre and posttest density values for all hydrostatic samples.

Table 4: Density values for all hydrostatic samples.

		Density (g/cc)		
Sample	Material	Pretest	Posttest	Comments
WC-HC-50-01	50%	1.88	2.48	
WC-HC-50-02	50%	1.89	2.55	
WC-HC-50-03	50%	1.9	2.75*	Jacket leak at 15MPa
WC-HC-50-04	50%	1.93	2.62	Pressure ramped directly to 5MPa
(asterisk values not included in average)		1.9	2.55	Average 50%
WC-HC-100-01	100%	2.08	2.52	
WC-HC-100-02	100%	2.12	2.66**	Pressure vessel leaked above 5MPa
WC-HC-100-03	100%	2.13	2.52	Pore pressure tube pinched off above 5MPa
WC-HC-100-04	100%	2.12	2.68**	Pressure vessel leaked
WC-HC-100-05	100%	2.14	2.53	
(asterisk values not included)		2.12	2.52	Average 100%
*Note: Posttest density from sample WC-HC-50-03 is likely inaccurate due to jacket leak and resulting in a heavier posttest sample weight.				
**Note: Posttest density is likely inaccurate due to a leak in the pressure vessel resulting in an inaccurate post compaction volume measurement				

6.2 Triaxial Tests

Ten triaxial tests were performed on 50% degraded material and nine triaxial tests were performed on 100% degraded material. Confining pressures were 1, 2, 5, and 15 MPa.

Based on initial hand measurements of each sample after die compaction to 80% of target confining pressure, Table 5 lists the density for each triaxial sample at three different stages during the test; 1) post die compaction, 2) post overnight hydrostatic hold, and 3) post triaxial test. To compute sample density after the overnight hydrostatic hold, fluid was captured and weighed and volume strain was determined from axial and radial displacement transducers mounted directly on the sample.

Two samples, WC-TX-50-02-02 and WC-TX-50-02-04, were die compacted to 1.8 MPa or 90% of target hydrostatic confining pressure as opposed to 80% for all other samples. While these samples exhibit overall higher Young's modulus values throughout the test, the data appears within the expected scatter based on other tests at different confining pressures. Thus these samples are included in the analyses.

A typical plot of true differential stress versus true strain is shown in Figure 19 and represents a test on 100% degraded material. Note that a peak stress is observed; a feature most commonly seen on the 100% degraded material. All 50% degraded tests except for tests at 15 MPa confining pressure did not reach a peak stress value. Peak stress values for the 100% degraded material are shown in Figure 20 and plotted versus confining pressure. This plot presents the data in a Mohr-Coulomb manner and gives an idea of the failure surface for the material.

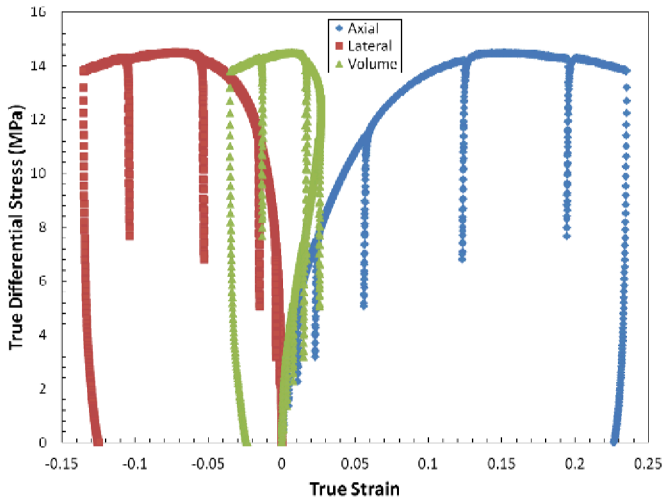

Fig. 19. Typical plot of true differential stress versus true strain from a 100% degraded material triaxial test.

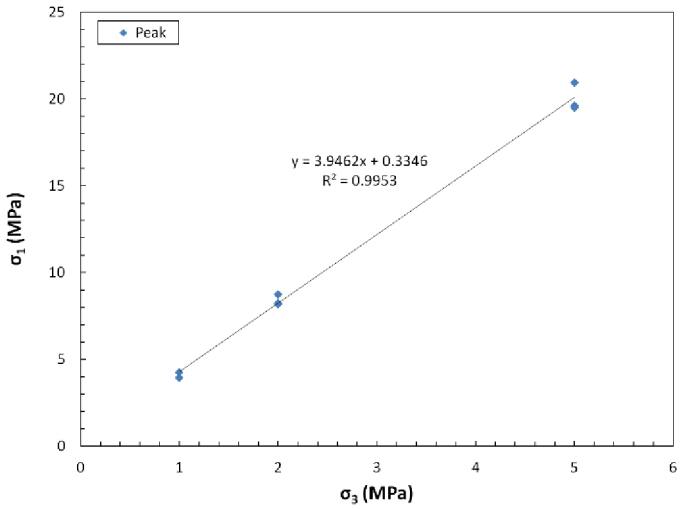

Fig. 20. Plot of σ_1 versus σ_3 (peak strength values) for all 100% degraded material tests.

Table 5: Density values all triaxial samples.

Sample	Density post die compaction (g/cc)	Density post overnight hydrostatic hold (g/cc)	Density post triax test (g/cc)
WC-TX-50-01-01	2.02	2.2	2.29
WC-TX-50-01-02	2.09	2.26	2.27
WC-TX-50-02-01	1.99	No Test	
WC-TX-50-02-02	2.07	2.35	2.43
WC-TX-50-02-03	2	No Test	
WC-TX-50-02-04	2.07	2.35	2.38
WC-TX-50-02-05	2.08	No Test	
WC-TX-50-02-06	2.05	2.31	2.31
WC-TX-50-05-01	2.2	2.49	2.52
WC-TX-50-05-02	2.11	2.42	2.43
WC-TX-50-05-03*	2.07	2.41	2.37
WC-TX-50-15-01	2.14	No Test	
WC-TX-50-15-02	2.18	2.61	2.61
WC-TX-50-15-03	2.15	2.62	2.56
WC-TX-100-01-01	2.28	2.36	2.25
WC-TX-100-01-02	2.28	2.35	2.22
WC-TX-100-02-01	2.32	2.46	2.39
WC-TX-100-02-02	2.29	2.39	2.37
WC-TX-100-02-03**	2.34	N/A	2.39
WC-TX-100-05-01	2.33	2.48	2.48
WC-TX-100-05-02	2.31	2.49	2.4
WC-TX-100-05-04*	2.26	2.23	N/A
WC-TX-100-05-05*	2.36	2.51	2.58
*Slow test (20 times slower than other tests)			
**Sample barreling investigated (Lateral LVDT's mounted at midheight and 25% from one end)			

From the internal sample mounted LVDT's, Young's modulus and Poisson's ratio were determined as a function of axial strain. Young's modulus results are presented graphically in Figure 21 and Figure 22 for 50% and 100% degraded material respectively. Poisson ratio values are not shown for triaxial tests due to erroneous high values. An investigation was conducted that included running tests on each material type at pressurization and axial strain rates 20 times slower than used in the other tests. This change in rates did not give a change in Poisson ratio values. It was decided that sample barreling was occurring from the results of changing the location of the lateral LVDT's (one gage mounted at sample midheight and one 25% from one end). The LVDT mounted 25% from one end gave significantly smaller lateral strains than the LVDT mounted at sample midheight. It was concluded that lateral strain was a function of location along the length of the sample. Tests with asterisk markers next to them in Table 5, Figure 21, and Figure 22 are tests run with different rates and transducer configuration as described in the aforementioned sample barreling investigation. These erroneous Poisson ratio values from the triaxial test series was the motivator for conducting the uniaxial strain tests discussed in Section 6.3.

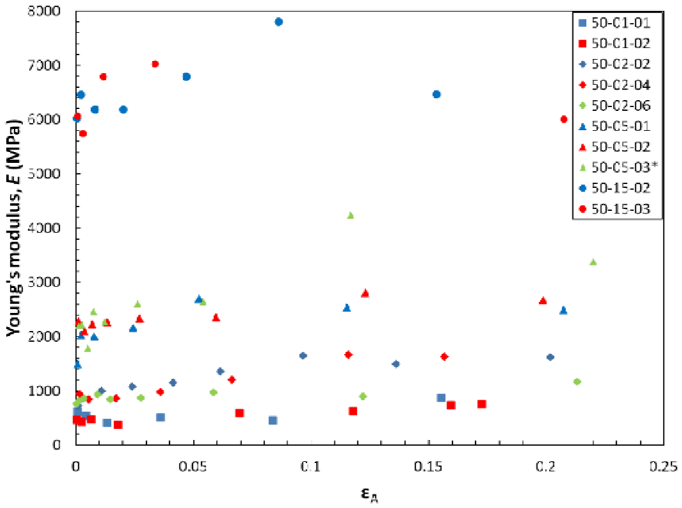

Fig. 21. Young's modulus versus axial strain for all 50% degraded material triaxial tests. The "*" in the legend is the same note as in Table 5.

Bulk modulus values were determined after the overnight hydrostatic hold prior to the application of differential stress. Volumetric strain was calculated from equation (2) using the sample mounted LVDT's. These values are compared to the average bulk modulus values from the hydrostatic test series and compare reasonably well at lower confining pressures. At higher confining pressures (5 and 15 MPa) bulk modulus values determined using sample mounted LVDT's are lower than bulk modulus values determined using dilatometry (hydrostatic test series). This discrepancy could be a result of two factors: 1) lateral strain measurement taken

at two discreet points along the length of the sample (see sample barreling investigation presented earlier in this section) and 2) the limitation of resolution of dilatometry measurements at higher confining pressures.

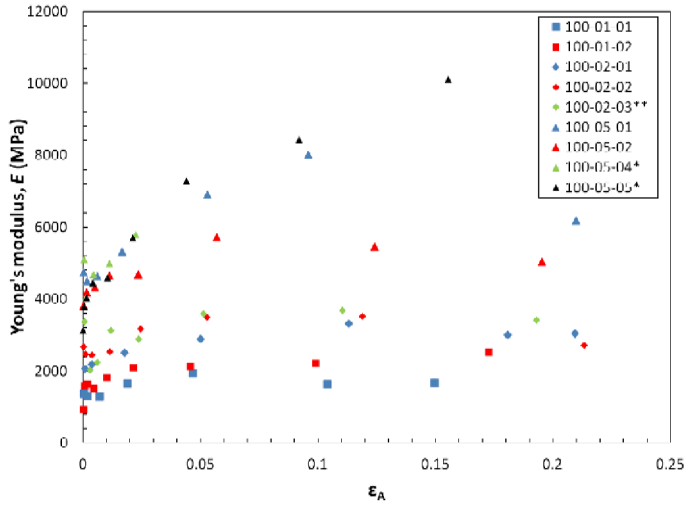

Fig. 22. Young's modulus versus axial strain for all 100% degraded material triaxial tests. The "*" and "**" in the legend are the same notes as in Table 5.

6.3 Uniaxial Strain tests

Figure 23 shows a typical plot of radial stress versus axial stress where the slope of the line gives Poisson's ratio from equation (14). Once Poisson's ratio is known, Young's modulus can be calculated from equation (20). The slope of the line in equation (20) is represented by a plot of true differential stress versus true axial strain (Figure 24).

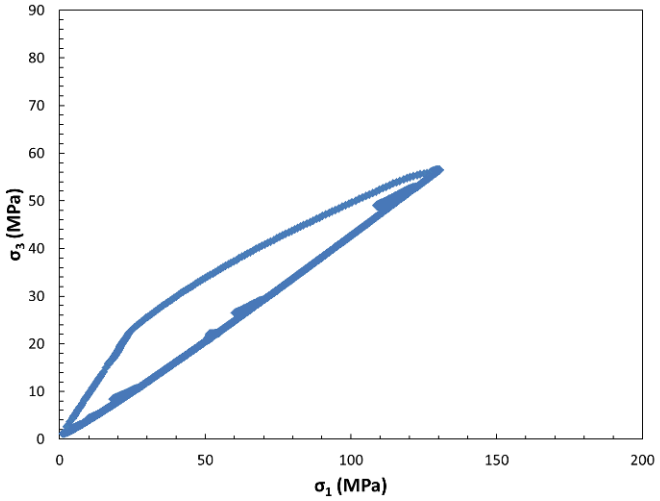

Fig. 23. Typical plot of confining pressure versus axial stress where the slope gives Poisson's ratio.

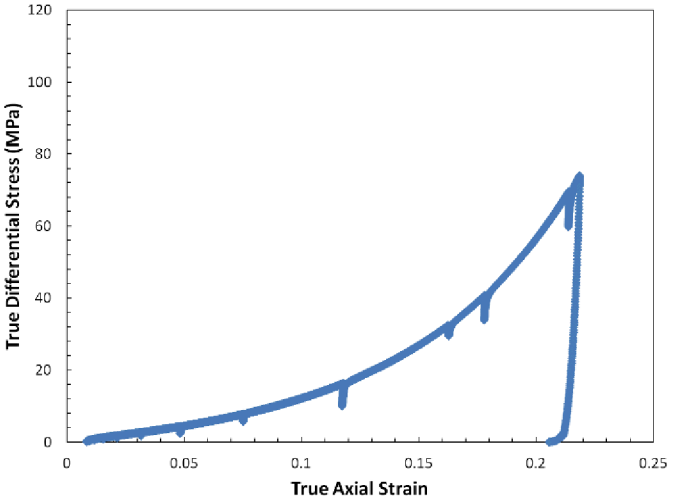

Fig. 24. Typical plot of true differential stress versus true axial strain where once Poisson's ratio is known, the slope gives Young's modulus.

With lateral strain held at zero, sample volume for uniaxial strain tests was calculated directly from axial strain measurements. Weight of the sample at each unload/reload loop was determined by weighing brine expelled from the sample. These measurements allow us to determine Young's modulus and Poisson's ratio as a function of density. These relationships are shown for both 50% and 100% degraded materials in Figures 25 and 26 respectively. Densities for both materials range between 2.2 g/cc to 2.9 g/cc. Young's modulus increases gradually up to a density of ~2.5g/cc after which the samples stiffen at a faster rate. Poisson's ratio also increases with increasing density, but the increase is more subtle than with Young's modulus. At the highest density measured, Poisson's ratio is ~0.35 and ~0.25 for 50% and 100% degraded materials, respectively. Young's modulus values and densities obtained from uniaxial strain testing more than cover the range of values obtained during triaxial testing. Young's modulus is much higher for all densities measured for the 100% degraded material.

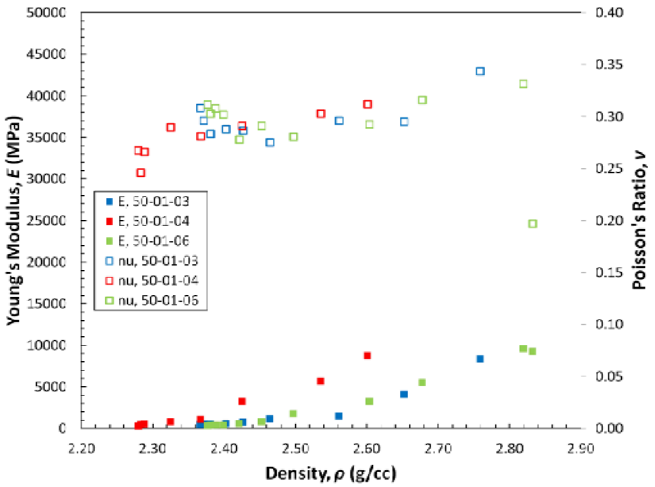

Fig. 25. Young's modulus and Poisson's ratio versus density for 50% degraded material uniaxial strain tests.

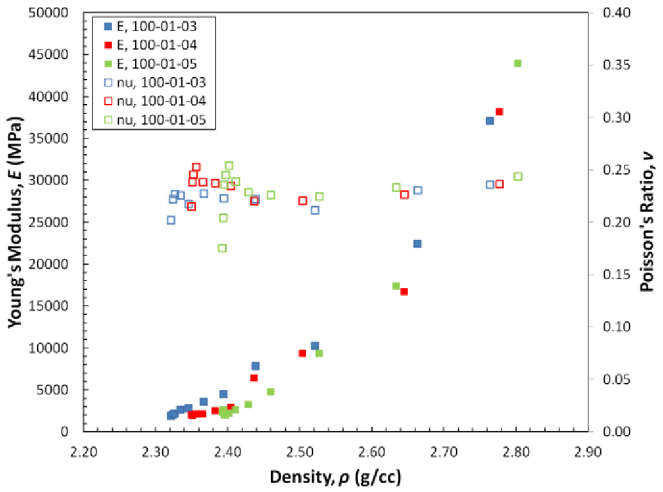

Fig. 26. Young's modulus and Poisson's ratio versus density for 100% degraded material uniaxial strain tests.

7. CONCLUSIONS

A test suite was conducted that established the following for two surrogate material recipes representing 50% and 100% degraded waste states at the WIPP:

- Bulk modulus was determined as a function of confining pressure
- Young's modulus and Poisson's ratio were determined as a function of density
- The effect of pore pressure was investigated
- A Mohr-Coulomb failure envelope was developed from 100% degraded triaxial tests

In some cases, novel test methods and equipment were developed to handle the unique material composition. Included was the following: 1) use of a dual piston dilatometer system capable of handling large volumetric strains while still giving the precision necessary for reliable bulk modulus measurements, 2) dual LVDT radial displacement rings to allow for measurement of large radial sample displacements within the limited confines of a pressure vessel and 3) uniaxial strain condition using confining pressure to maintain zero lateral strain allowing determination of Young's modulus and Poisson's ratio as a function of sample density. This work was funded by DOE through WIPP programs.

Sandia National Laboratories is a multi-program laboratory managed and operated by Sandia Corporation, a wholly owned subsidiary of Lockheed Martin Corporation, for the U.S. Department of Energy's National Nuclear Security Administration under contract DE-AC04-94AL85000.

This research is funded by WIPP programs administered by the Office of Environmental Management (EM) of the U.S Department of Energy.

REFERENCES

1. Hansen, F.D., Knowles, M.K., Thompson, T.W., Gross, M., McLennan, J.D., Schatz, J.F., 1997. Description and Evaluation of a Mechanistically Based Conceptual Model for Spall, *SAND97-1369*, Sandia National Laboratories, Albuquerque, NM.
2. Fung, Y.C., 1993. *A First Course in Continuum Mechanics*, 3rd ed., Prentice-Hall, Inc.